How to cite:
doi.org/10.1002/anie.202300186

Metal-Organic Frameworks Hot Paper

Near IR Bandgap Semiconducting 2D Conjugated Metal-Organic Framework with Rhombic Lattice and High Mobility

Lukas Sporrer[+], Guojun Zhou[+], Mingchao Wang[+], Vasileios Balos, Sergio Revuelta, Kamil Jastrzembski, Markus Löffler, Petko Petkov, Thomas Heine, Angieszka Kuc, Enrique Cánovas,* Zhehao Huang,* Xinliang Feng,* and Renhao Dong**

Abstract: Two-dimensional conjugated metal–organic frameworks (2D *c*-MOFs) are emerging as a unique class of electronic materials. However, 2D *c*-MOFs with band gaps in the Vis-NIR and high charge carrier mobility are rare. Most of the reported conducting 2D *c*-MOFs are metallic (i.e. gapless), which largely limits their use in logic devices. Herein, we design a phenanthrotriphenylene-based, D_{2h}-symmetric π-extended ligand (**OHPTP**), and synthesize the first rhombic 2D *c*-MOF single crystals (**Cu_2(OHPTP)**). The continuous rotation electron diffraction (cRED) analysis unveils the orthorhombic crystal structure at the atomic level with a unique slipped AA stacking. The **Cu_2(OHPTP)** is a *p*-type semiconductor with an indirect band gap of ≈0.50 eV and exhibits high electrical conductivity of 0.10 S cm^{-1} and high charge carrier mobility of ≈10.0 cm^2 V^{-1} s^{-1}. Theoretical calculations underline the predominant role of the out-of-plane charge transport in this semiquinone-based 2D *c*-MOF.

Introduction

Metal-organic frameworks (MOFs) are a versatile class of coordination polymers with high crystallinity, large surface areas and pore volumes that have attracted considerable attention in a wide variety of fields, such as gas storage and separation, sensing and catalysis.[1] However, most of the three-dimensional (3D) MOFs developed to date are electrical insulators, limiting their application in areas that require long-range charge transport, such as electronics.[2] To fill this gap, two-dimensional conjugated MOFs (2D *c*-MOFs), which refer to a class of layer-stacked MOFs with in-plane extended π-conjugation and out-of-plane π–π stacking interactions, have emerged and exhibited uniquely record-high electrical conductivities (up to 10^3 S cm^{-1}).[3] In 2012, the first 2D *c*-MOF was reported by linking C_3 symmetric hexahydroxytriphenylene (HHTP) via metal-O_4 (MO_4) linkages.[4] Since then, various planar, C_6 (e.g. benzene, coronene),[5] C_3 (e.g. triphenylene)[6] or C_4 symmetric (e.g. phthalocyanine)[7] conjugated ligands containing ortho-substituted linking groups (e.g. OH, NH_2, SH, SeH) have been developed for the construction of 2D *c*-MOFs. Owing to the abundant, well-defined metal-heteroatom coordination sites, intrinsic electrical conductivity, redox activity and porosity, the novel subclass of 2D *c*-MOFs have attracted substantial interest in opto-electronics,[8] spintronics,[9] and energy storage devices.[10]

While being good electrical conductors, most of the reported 2D *c*-MOFs exhibit a gapless electronic band structure.[11] Till now, only a few semiquinone-based (MO_4-linked) 2D *c*-MOFs with honeycomb or square lattice have

[*] L. Sporrer,[+] Dr. M. Wang,[+] K. Jastrzembski, Prof. T. Heine, Prof. Dr. X. Feng, Prof. Dr. R. Dong
Chair of Molecular Functional Materials, Faculty of Chemistry and Food Chemistry, Technische Universität Dresden
Mommsenstrasse 4, 01062 Dresden (Germany)
E-mail: xinliang.feng@tu-dresden.de

Dr. G. Zhou,[+] Dr. Z. Huang
Department of Materials and Environmental Chemistry, Stockholm University
10691 Stockholm (Sweden)
E-mail: zhehao.huang@mmk.su.se

Dr. V. Balos, S. Revuelta, Prof. Dr. E. Cánovas
Instituto Madrileño de Estudios Avanzados en Nanociencia (IMDEA Nanociencia)
28049 Madrid (Spain)
E-mail: enrique.canovas@imdea.org

Dr. M. Löffler
Dresden Centre for Nanoanalysis, Technische Universität Dresden
Helmholtzstr. 18, 01062 Dresden (Germany)

Prof. Dr. P. Petkov
University of Sofia, Faculty of Chemistry and Pharmacy
1164 Sofia (Bulgaria)

Dr. A. Kuc
Helmholtz-Zentrum Dresden-Rossendorf, Abteilung Ressourcenökologie, Forschungsstelle Leipzig
04318 Leipzig (Germany)
E-mail: a.kuc@hzdr.de

Prof. Dr. X. Feng
Max-Planck-Institut für Mikrostrukturphysik
Weinberg 2, 06120 Halle (Germany)

Prof. Dr. R. Dong
Key Laboratory of Colloid and Interface Chemistry of the Ministry of Education, School of Chemistry and Chemical Engineering, Shandong University
Jinan, 250100 (China)
E-mail: renhaodong@sdu.edu.cn

[+] These authors contributed equally to this work.

been discovered to be intrinsic semiconductors, but exhibiting relatively low charge-carrier mobilities of below $\approx 5\ cm^2\ V^{-1}\ s^{-1}$.[12] This limits the performance of 2D *c*-MOFs in logic devices, where an appreciable finite band gap in needed. Therefore, it is highly attractive to develop novel 2D *c*-MOF semiconductors with wider band gaps, large carrier mobilities and high porosities.[13]

Herein, we address this challenge by designing a planar, conjugated ligand, 2,3,6,7,11,12,15,16-octahydroxyphenanthro[9,10:*b*]triphenylene (**OHPTP**) with D_{2h}-symmetry and four connecting points. From this unique π-extended ligand, we have further prepared an OHPTP-based CuO_4-linked 2D *c*-MOF, **Cu_2(OHPTP)**, which is the first example of a rhombic single-crystalline 2D *c*-MOF. Notably, these porous samples (surface area up to $741\ m^2 g^{-1}$) can be obtained as single crystals with rod-like morphology with lengths in the μm range and widths of several hundred nanometers. The rhombic crystal structure of **Cu_2(OHPTP)** was resolved using continuous rotation electron diffraction (cRED) at the atomic level, providing a slipped AA layer-stacking sequence. Density-functional theory (DFT) calculations of the electronic structures of **Cu_2(OHPTP)** reveal that the band dispersion is preferred in the out-of-plane direction, causing this sample to be semiconducting with an indirect band gap of ≈0.50 eV. This **Cu_2(OHPTP)** 2D *c*-MOF displays a relatively high conductivity of $0.10\ S\,cm^{-1}$ at room temperature by the 4-probe method, that is further validated by terahertz time-domain spectroscopy (THz-TDS) in the AC limit. It is noteworthy that THz spectroscopy reveals a charge carrier mobility as high as $\approx 10.0\ cm^2\ V^{-1}\ s^{-1}$ and a density of $\approx 5\times10^{16}\ cm^{-3}$ under ambient conditions. The achieved mobility is primarily limited by grain boundary scattering (i.e. that will be dramatically boosted to several hundreds of $cm^2\ V^{-1}\ s^{-1}$ in larger crystals). These charge transport Figures, conductivity and mobility, of merit are far superior when compared to those reported for semiquinone-based 2D *c*-MOFs.[14]

Results and Discussion

OHPTP was prepared through a three-step synthesis with an overall yield of 79 %. After a fourfold Suzuki coupling of 1,2,4,5-tetrabromobenzene with 3,4-dimethoxyphenylboronic acid, the phenanthro[9,10:*b*]triphenylene (**PTP**) core was then constructed by a $FeCl_3$-promoted Scholl reaction. Finally, BBr_3 was employed to deprotect the eight methoxy groups on **PTP** yielding **OHPTP** as a light-green solid (Figure 1a, Scheme S1, detailed synthetic conditions are shown in Supporting Information).

Then, **Cu_2(OHPTP)** was solvothermally synthesized as a black powder by coordination between **OHPTP** and copper acetate in a mixed solvent of water and DMF (7:3) at 85 °C for 24 h (Figure 1a, see the optimization of copper source, solvents and temperature in Scheme S2 and Figure S1). Scanning electron microscopy (SEM) image indicates that the bulk **Cu_2(OHPTP)** 2D *c*-MOF consists of homogeneous rod-like single-crystals with lengths in the μm range and widths of several hundreds of nanometers (Figure 1b).

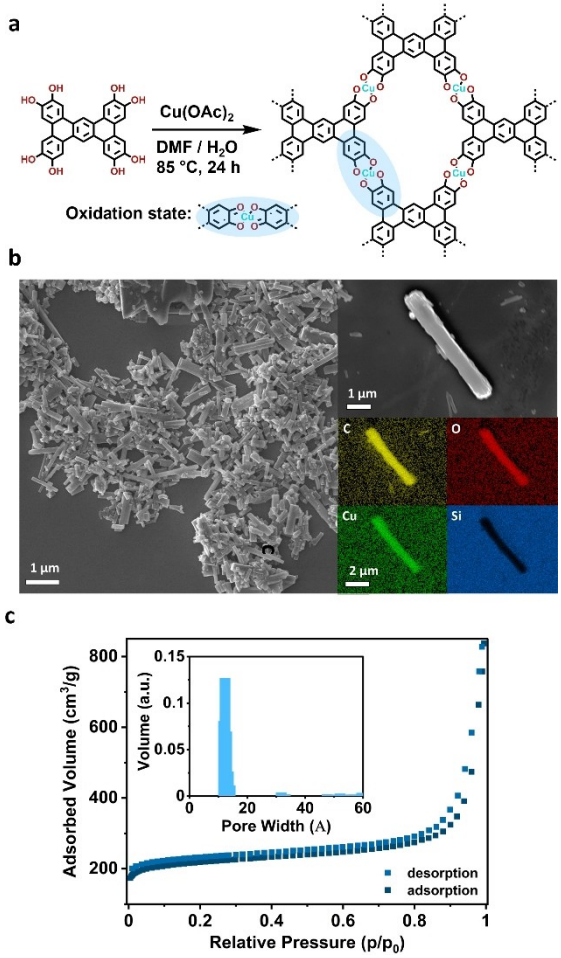

Figure 1. a) Synthetic Scheme of **Cu_2(OHPTP)**. b) SEM and EDX images of **Cu_2(OHPTP)** crystals. c) N_2 adsorption-desorption isotherm with the pore size distribution as the inset.

Energy dispersive X-ray (EDX) spectroscopy of a single crystal shows a uniform distribution of copper, carbon and oxygen elements throughout the sample (Figure 1b).

Fourier-transform infrared (FT-IR) spectrum depicts the disappearance of the O–H stretching vibration of **OHPTP** at 3000–3500 cm^{-1} in **Cu_2(OHPTP)**, indicating the successful coordination (Figure S2a). Raman spectroscopy reveals two characteristic bands: a broad one at 1350–1400 cm^{-1} and another one at ca. 1575 cm^{-1} (Figure S2b), which are similar to the D and G bands observed in graphene or graphite samples, respectively.[15] X-ray photoemission spectroscopy (XPS) confirms the presence of copper, oxygen and carbon in the sample (Figure S3). High-resolution O 2p XPS shows two oxygen peaks at 531.7 and 533.2 eV, corresponding to the ligand in the semiquinone form.[16] This is further confirmed by the analysis of C 1s spectrum that displays distinct C=C, C–O and C=O signals at 284.7, 286.2 and 288.6 eV, respectively.[17] The Cu 3d spectrum reveals the dominant presence of Cu^{II} in **Cu_2(OHPTP)** at a binding energy of 934.6 eV. Inductively coupled plasma optical emission spectroscopy (ICP-OES) coupled with elemental analysis (EA) suggests a Cu/C ratio of 0.37 in the

synthesized **Cu_2(OHPTP)** (Table S1), which agrees well with the proposed ratio of 0.35 for the chemical structure shown in Figure 1a.

Nitrogen adsorption-desorption measurement at 77 K indicated the nanoporous nature of **Cu_2(OHPTP)**. The Brunauer–Emmett–Teller (BET) surface area was determined to be 741 $m^2 g^{-1}$ with an estimated average pore size of about 1.23 nm (Figure 1c). Furthermore, **Cu_2(OHPTP)** is thermally stable up to 300 °C as revealed by thermogravimetric analysis (TGA) in an argon atmosphere (Figure S4). TGA also shows a weight loss of about 7 % at 100–150 °C, revealing the presence of tightly bound water molecules in the 2D *c*-MOF sample (i.e., three water molecules per structural unit). Taking the results of ICP-OES and EA (Table S1) into consideration, we calculated a chemical formula of $Cu_2(C_{30}H_8O_8)(H_2O)_3$ for **Cu_2(OHPTP)**. The electron paramagnetic resonance (EPR) spectrum depicts a broad signal at g = 2.122 that can be attributed to the unpaired Cu(d^9) electrons (Figure S5). Superconducting quantum interference device (SQUID) magnetic-susceptibility measurements indicate a linear $1/\chi$–T dependence, a characteristic for paramagnetic materials (Figure S6). The curve could be fitted to a Curie–Weiss law with $\theta = -1.98$ K, which is indicative of antiferromagnetic interactions between the neighboring metal nodes.[18]

We then investigated the crystal structure of **Cu_2(OHPTP)** by powder X-ray diffraction (PXRD), high-resolution transmission electron microscopy (HRTEM) and cRED. PXRD pattern exhibits prominent 2θ peaks at 5.8°, 8.0°, 11.6°, 12.6° 17.9° and 28.1° (Figure S7) corresponding to the d-spacing of 1.53, 1.10, 0.76, 0.70, 0.50 and 0.32 nm, respectively. The crystalline nature of **Cu_2(OHPTP)** was further studied by HRTEM. The out-of-plane HRTEM image and related fast Fourier transform (FFT) analysis (Figure 2a) indicate a long-range order across the whole rod crystallite along the z-axis with an interlayer distance of 0.31 nm. After delaminating the rod crystals into nanosheets, Figure 2b unambiguously reveals the rhombic topology of **Cu_2(OHPTP)** with *d* spacings of 1.54 and 1.11 nm, which fit well with those deduced from PXRD.

To determine the structure of **Cu_2(OHPTP)** at the atomic level, we measured cRED.[19] The cRED data provides unit cell parameters of $a = 22.74$ Å, $b = 21.58$ Å, $c = 6.50$ Å, $\alpha = 89.33°$, $\beta = 89.10°$, and $\gamma = 90.53°$, corresponding to the orthorhombic crystal system (Figure S9). The 3D reciprocal lattice and 2D planes indicate the following reflection conditions: *hkl*: $h+k=2n$; 0*kl*: $k=2n$; *h*0*l*: h, $l=2n$; and *hk*0: $h+k=2n$ (Figure 2c). The structure is therefore solved in the space group Cmcm (Supporting Information for detailed procedure).[20] Pawley fitting of the structure against the experimental PXRD converges to cell parameters of $a = 22.598(2)$ Å, $b = 21.581(3)$, and $c = 6.379(4)$ Å ($R_P = 4.419$, $R_{WP} = 5.891$, $R_{exp} = 2.710$, Goodness of fit (GOF) = 2.158) and offers an excellent fit for the recorded PXRD pattern (Figures 2f and S9). The observed diffractions could be indexed as 110, 200/020, 220, 310/130

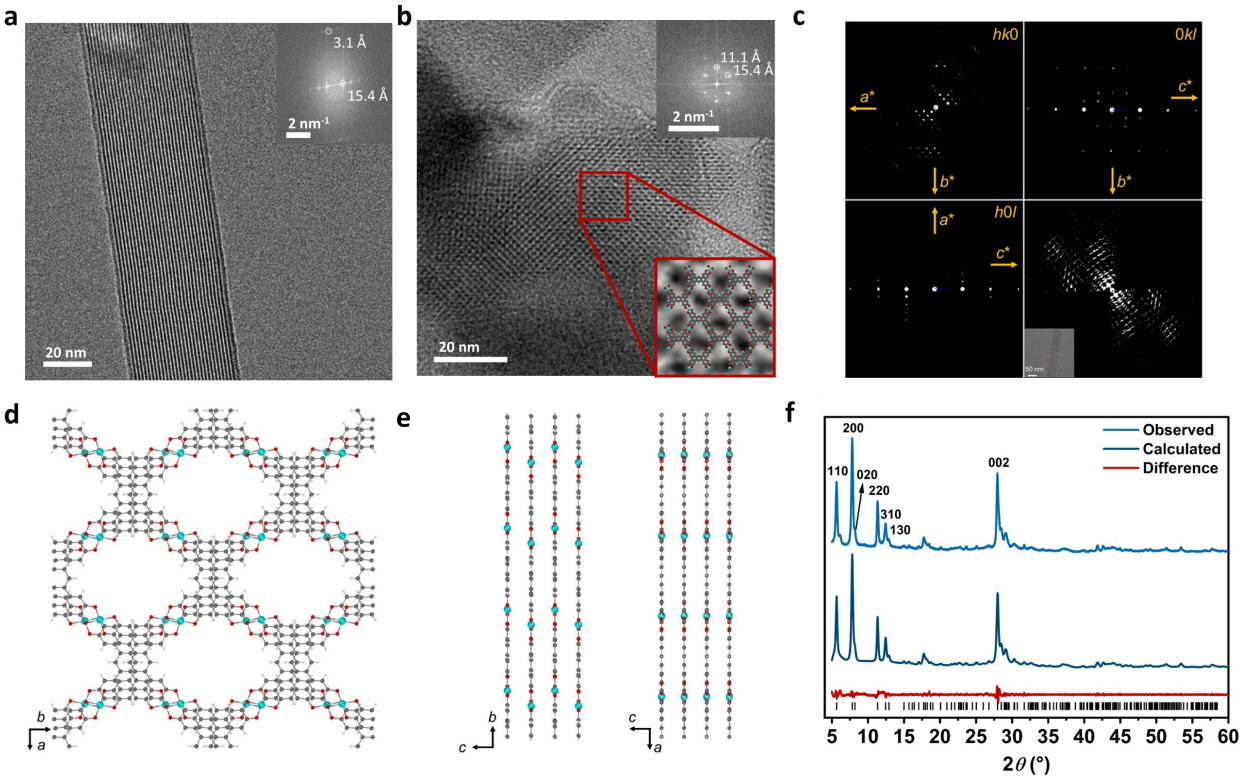

Figure 2. a) Out-of-plane and b) in-plane HR-TEM images with Fourier transformed electron diffractions and structure overlay as insets. c) Reconstructed 3D reciprocal lattice and 2D slide cuts from cRED data. d), e) In-plane and out-of-plane structure models, respectively. f) Experimental and Pawley-refined PXRD patterns.

and 002 planes for the diffractions at 5.8°, 8.0°, 11.6°, 12.6° and 28.1°, respectively. Notably, the solved structure confirms the formation of square-planar CuO_4 linkage between two **OHPTP** ligands; each of them is surrounded by four CuO_4 units to form the rhombic 2D **Cu_2(OHPTP)** network (Figure 2d). Moreover, the **Cu_2(OHPTP)** layers adopt an alternating stacking order (with an interlayer distance of 0.32 nm) where two layers are shifted along the b-axis with an offset close to 2 Å (Figure 2e). The slipped AA stacking results in an overlap of the aromatic cores while preventing a direct stacking of Cu atoms. The position of the metal nodes leads to a distorted pseudo-octahedral coordination environment of the Cu atoms (Figure 2d); the CuO_4 units are located in the equatorial position with Cu–O bond lengths of 2.0 and 1.9 Å, while two additional, axial oxygen atoms from the adjacent layers are present with a Cu–O distance of 3.2 Å.

The band structures of monolayer and bulk **Cu_2(OHPTP)** were calculated using DFT on the resolved crystal structure. After initial geometry optimization (relaxation of atomic positions; Supporting Information for detailed parameters), the band structure and electronic density-of-states (DOS) were calculated at the DFT/HSE06 level of theory with the POB-TZVP basis set as implemented in Crystal17. The monolayer presents a spin-paired state, and the band structure shows nearly flat bands with a gap of 0.75 eV. The DOS in the energy window of ±1.5 eV around the Fermi level (E_F) is mostly localized at the ligand or metal atoms, indicating a limited π-conjugation within the 2D plane (Figure 3a). In the layer-stacked case, the energetically most favorable spin state is a high-spin state with 16 unpaired electrons per unit cell, which also corresponds to the results of SQUID measurements. The unpaired spins are mainly localized at the Cu and O centers in the linkage.

The multilayered 2D *c*-MOF is a semiconductor with an indirect band gap of around 0.61 eV and 0.45 eV for alpha and beta spin channels, respectively (Figure 3b). Contrary to the monolayer, the band dispersion is more prominent and rather high in the out-of-plane direction. However, visible dispersion appears also in-plane upon stacking. The effective masses of the electron and holes in the VB and CB were calculated as $m_e = 0.78\, m_0$ and $m_h = 1.21\, m_0$ and the harmonic mean as $m^* = 0.96\, m_0$. The electronic states show high conjugation and hybridization between Cu, C and O atoms. As suggested from the calculations, the π-*d* orbital overlap leading to the electron delocalization is only visible in the bulk system supporting the importance of the stacking interactions and proximity effects on the overall transport properties previously calculated theoretically.[21]

Solid state UV/Visible-near IR (NIR) absorption spectrum of **Cu_2(OHPTP)** coated on quartz glass shows two strong absorption bands in the visible region with an absorption maximum at 320 and 620 nm, respectively, and one broad and weak band in the NIR range (Figure 4a). The first two bands can be ascribed to π–π* and metal-to-ligand charge transfer,[9] while the NIR absorption is the characteristic of highly-conjugated polymeric materials.[6a] The optical band gap was further determined to be ≈0.5 eV by the Tauc method for an indirect transition (Figure S10), comparable

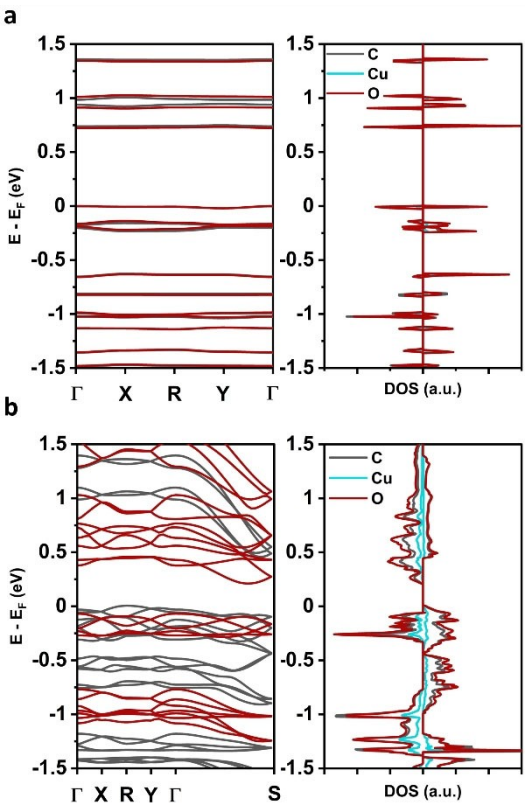

Figure 3. Band structure for alpha (black) or beta (red) spins and density of states (DOS) projected on atoms of **Cu_2(OHPTP)**. a) Monolayer and b) layered bulk model.

to the above calculated results. Ultraviolet-photoemission spectroscopy (UPS) was used to probe the energy of the valence band level with respect to the E_F (Figure 4b, Figure S11). No clear valence band maximum appeared under a bias of 5 V and a constant decrease of electron density up to the E_F was observed, indicating the presence of electronic states close to the E_F, suggesting strong *p*-type doping in the material.

To assess the electrical properties of **Cu_2(OHPTP)**, we pressed the MOF powders into a pellet, and measured its conductivity using the 4-probe method in the van-der-Pauw geometry under argon. The linear current–voltage curve confirms the Ohmic contact (Figure S12a). **Cu_2(OHPTP)** shows a nonlinear increase of conductivity with increasing temperature (Figure 4c, Figure S12b), indicating a typical semiconducting behavior where charge carrier transport is thermally activated. A conductivity of 0.1 $S\,cm^{-1}$ at 300 K could be determined. Fitting the conductivity-temperature plot by an Arrhenius-type function provides a thermal energy gap of ≈0.23 eV in the high-temperature region (Figure 4c). In the temperature range between 40 to 300 K, the conductivity data could be properly modelled by a 3D Mott variable range hopping model (Figure S12d). This indicates that hopping dominates the charge transport between different single crystals, which is often observed in polycrystalline samples (see Supporting Information).

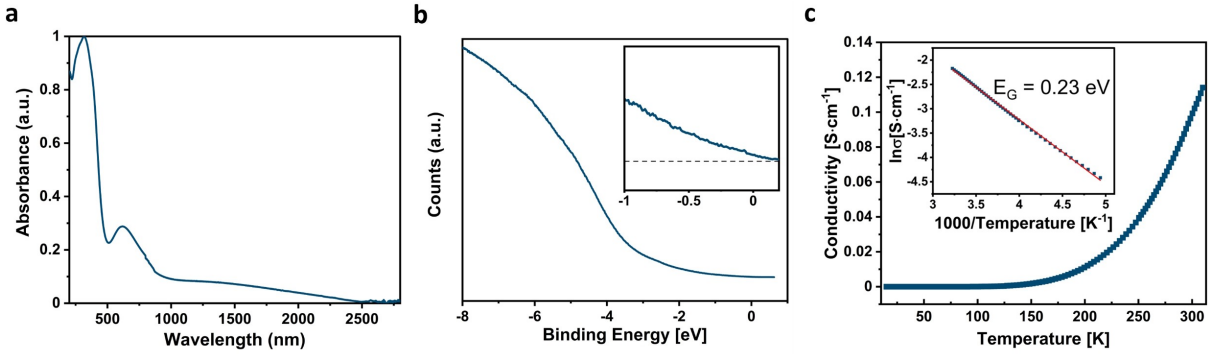

Figure 4. a) UV/Visible-NIR spectrum of **Cu_2(OHPTP)** on quartz glass. b) UPS of a thin layer of **Cu_2(OHPTP)** on gold coated SiO_2 with zoom on the Fermi energy. c) Van-der-Pauw variable temperature-conductivity measurement of the **Cu_2(OHPTP)** pellet sample. The Arrhenius plot is shown in an inset.

In order to investigate the charge carrier mobility and charge density in **Cu_2(OHPTP)**, we performed terahertz time-domain spectroscopy (THz-TDS). This technique probes the frequency-resolved complex conductivity of the sample in a non-contact fashion.[22] To access this information, a regular measurement compares the changes in amplitude and phase in transmission for a freely propagating ≈1 THz pulse through the air and the sample (Supporting Information for detailed conditions). The THz-TDS results on a 280 μm thick powder sample sandwiched between fused silica windows at 300 K are presented in Figure 5a. The conductivity of the sample can be properly described by the Drude–Smith (DS) model (see Supporting Information). This phenomenological model is applied to free carriers experiencing some degree of localization induced by backscattering, which is weighted by the backscattering parameter c_{DS} in the DS model (see Supporting Information).[23] The latter can take values between 0 and −1, representing a lack or total localization of free charge carriers within the probed mean free path, respectively. From the DS model,

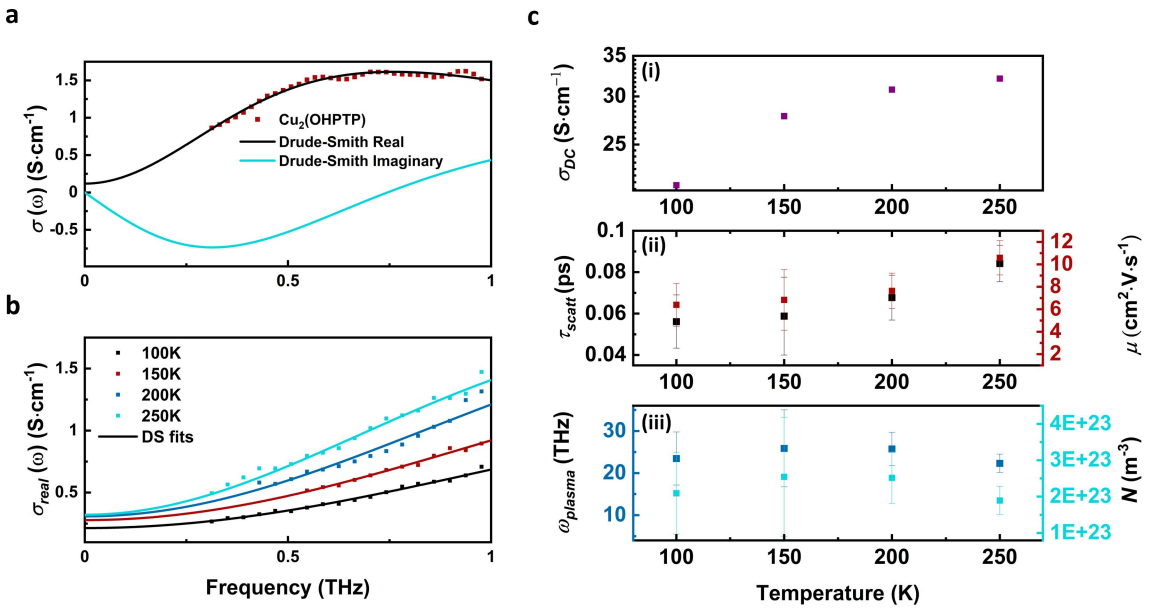

Figure 5. a) Frequency-resolved real conductivity of **Cu_2(OHPTP)** powder (thickness of 280 μm). The red solid squared data points correspond to the experimentally derived values under ambient conditions. The corresponding solid lines are best fit with the Drude–Smith model [see Eq. (S3)], giving access to the real (black solid line) and imaginary (blue solid line) conductivity. b) Frequency-resolved real conductivity of **Cu_2(OHPTP)** powder (thickness of 150 μm) with increasing temperature in vacuum conditions. The solid squared datapoints correspond to the experimentally derived values at 100 K (black), 150 K (red), 200 K (dark blue) and 250 K (light blue). The corresponding solid lines are fits to the Drude–Smith model [see Eq. (S1)]. c) (i) Static conductivity (σ_{DC}, purple), (ii) scattering time (τ_{scatt}, black) with the corresponding mobility (μ, red), calculated using Equation (S4) and (iii) plasma frequencies (ω_{plasma}, dark blue) with the corresponding carrier density (N, light blue), calculated using Equation (S5). The error bars for τ_{scatt} and ω_{plasma}, correspond to standard errors returned by the fitting routine, while the error bars for μ and N are calculated by standard error propagation.

we obtain a scattering time of $\tau_s = 0.205$ ps and a plasma frequency of $\omega_p = 13.28$ THz. Taking into account the effective mass of holes estimated theoretically for a p-type semiconductor ($m_h = 1.21\, m_0$) and the value $c = -0.97$ obtained from the DS fit, we can obtain a charge carrier mobility ($\mu = \left(\frac{\tau e}{m^*}\right)[1+c]$) and carrier (hole) density as $\mu \approx 10\ cm^2 V^{-1} s^{-1}$ and $N = 6.7 \times 10^{16}\ cm^{-3}$ respectively. The inferred value of charge carrier concentration is assigned to p-type charge carriers. The value obtained for the mobility is rather large taking into account that the obtained c_{DS} parameter almost equals 1; in this respect, if the DS model is accurate in describing the data, one could extrapolate the expected value for the mobility for a single crystal (for $c_{DS} = 0$) as $\mu = 299\ cm^2 V^{-1} s^{-1}$. Finally, it is worth highlighting here that the DC conductivity of the bulk sample extrapolated from the DS model to the zero-frequency limit ($\sigma_{DC} = 0.1\ S cm^{-1}$) matches the value obtained by using 4-probe contact techniques (Figure 4c); which seems to support the data and DS modelling.

To obtain information about the charge transport mechanism, we performed temperature-dependent THz-TDS experiments on **Cu_2(OHPTP)** powder sample (150 μm thick) under vacuum (see Supporting Information). From bare data (see Figures 5b and c(i)) we resolved a decay of the DC conductivity, in qualitative agreement with the 4-probe data. From DS modeling we obtain the T variation of the scattering rate and plasma frequency (Figure 5c (ii) and (iii)). While the plasma frequency of the sample and consequently the p-type charge carrier density remain largely unaffected by increasing temperature, the scattering times (and hence mobilities) increase with increasing temperature (see Figure 5c). This suggests a thermally activated hopping-type charge transport mechanism, consistent with the results obtained on DC probes. Finally, we need to note that the backscattering parameter c_{DS}, remains fairly constant for all temperatures (see Supporting Information, Figure S13).

Conclusion

In summary, we present a novel, single-crystalline, conductive 2D *c*-MOF with a unique rhombic topology. The **Cu_2(OHPTP)** is a p-type semiconductor with an indirect band gap of 0.5 eV and exhibits high room-temperature electrical conductivity of $0.1\ S cm^{-1}$. DFT calculations suggest that the large aromatic core of **OHPTP** leads to improved π–π interactions along the direction normal to the plane, which contributes to strong band dispersion close to the Fermi level and dominates the overall conductivity. Terahertz spectroscopy analysis demonstrated a high charge mobility of $\approx 10.0\ cm^2 V^{-1} s^{-1}$ which represented a record among the semiquinone-based 2D *c*-MOFs. Our work paves the path to the development of high-mobility semiconducting MOFs for future logic devices.

Acknowledgements

This work is financially supported by the ERC starting grant (FC2DMOF, No. 852909), ERC Consolidator Grant (T2DCP, No. 819698), DFG project (CRC-1415, No. 417590517), EMPIR-20FUN03-COMET, as well as the German Science Council and Center for Advancing Electronics Dresden (cfaed). R.D. thanks Taishan Scholars Program of Shandong Province (tsqn201909047) and the National Natural Science Foundation of China (22272092). E.C. acknowledges MCIN/AEI grant PID2019-107808RA-I00 and Comunidad de Madrid grants 2021–5A/AMB-20942 & P2018/NMT-451. V.B. acknowledges MSCA HORIZON 2020 funding via 101030872 – PhoMOFs grant. Z.H. acknowledges financial support from the Swedish Research Council Formas (2020-00831), and the Swedish Research Council (VR, 2022–02939). We thank Zichao Li and Yunxia Zhou (HZDR Dresden-Rossendorf) for conductivity and SQUID measurements, Marielle Deconinck (TU Dresden) for UPS measurements, Darius Pohl (DCN) for TEM analysis and Yannan Liu (TU Dresden) for initial structure modeling. We acknowledge the use of the facilities at the Dresden Center for Nanoanalysis at Technische Universität Dresden. The authors thank the Center for Information Services and High-Performance Computing (ZIH) at TU Dresden for generous allocations of computer time.

Conflict of Interest

The authors declare no conflict of interest.

Data Availability Statement

The data that support the findings of this study are available from the corresponding author upon reasonable request.

Keywords: 2D Conjugated MOFs · Coordination Polymers · High Mobility · Semiconductors · Single Crystals

[1] a) O. M. Yaghi, N. W. Ockwig, H. K. Chae, M. Eddaoudi, J. Kim, *Nature* **2003**, *423*, 705; b) R. J. Kuppler, D. J. Timmons, Q.-R. Fang, J.-R. Li, T. A. Makal, M. D. Young, D. Yuan, D. Zhao, W. Zhuang, H.-C. Zhou, *Coord. Chem. Rev.* **2009**, *253*, 3042; c) A. H. Chughtai, N. Ahmad, H. A. Younus, A. Laypkov, F. Verpoort, *Chem. Soc. Rev.* **2015**, *44*, 6804.
[2] M. Wang, R. Dong, X. Feng, *Chem. Soc. Rev.* **2021**, *50*, 2764.
[3] a) M. Ko, L. Mendecki, K. A. Mirica, *Chem. Commun.* **2018**, *54*, 7873; b) L. S. Xie, G. Skorupskii, M. Dinca, *Chem. Rev.* **2020**, *120*, 8536.
[4] M. Hmadeh, Z. Lu, Z. Liu, F. Gándara, H. Furukawa, S. Wan, V. Augustyn, R. Chang, L. Liao, F. Zhou, E. Perre, V. Ozolins, K. Suenaga, X. Duan, B. Dunn, Y. Yamamto, O. Terasaki, O. M. Yaghi, *Chem. Mater.* **2012**, *24*, 3511.
[5] a) T. Kambe, R. Sakamoto, K. Hoshiko, K. Takada, M. Miyachi, J. H. Ryu, S. Sasaki, J. Kim, K. Nakazato, M. Takata, H. Nishihara, *J. Am. Chem. Soc.* **2013**, *135*, 2462; b) J. Park, A. C. Hinckley, Z. Huang, D. Feng, A. A. Yakovenko, M. Lee, S. Chen, X. Zou, Z. Bao, *J. Am. Chem. Soc.* **2018**, *140*, 14533;

c) N. Lahiri, R. Tsuchikawa, V. V. Deshpande, J. Louie, *J. Am. Chem. Soc.* **2017**, *139*, 19; d) R. Dong, Z. Zhang, D. C. Tranca, S. Zhou, M. Wang, P. Adler, Z. Liao, F. Liu, Y. Sun, W. Shi, Z. Zhang, E. Zschech, S. C. B. Mannsfeld, C. Felser, X. Feng, *Nat. Commun.* **2018**, *9*, 2637.

[6] a) D. Sheberla, L. Sun, M. A. Blood-Forsythe, S. Er, C. R. Wade, C. K. Brozek, A. Aspuru-Guzik, M. Dincă, *J. Am. Chem. Soc.* **2014**, *136*, 8859; b) A. J. Clough, J. W. Yoo, M. H. Mecklenburg, S. C. Marinescu, *J. Am. Chem. Soc.* **2015**, *137*, 118; c) Y. Cui, J. Yan, Z. Chen, W. Xing, C. Ye, X. Li, Y. Zou, Y. Sun, C. Liu, W. Xu, D. Zhu, *iScience* **2020**, *23*, 100812; d) J. H. Dou, M. Q. Arguilla, Y. Luo, J. Li, W. Zhang, L. Sun, J. L. Mancuso, L. Yang, T. Chen, L. R. Parent, G. Skorupskii, N. J. Libretto, C. Sun, M. C. Yang, P. V. Dip, E. J. Brignole, J. T. Miller, J. Kong, C. H. Hendon, J. Sun, M. Dincă, *Nat. Mater.* **2021**, *20*, 222.

[7] a) M. Wang, H. Shi, P. Zhang, Z. Liao, M. Wang, H. Zhong, F. Schwotzer, A. S. Nia, E. Zschech, S. Zhou, S. Kaskel, R. Dong, X. Feng, *Adv. Funct. Mater.* **2020**, *30*, 2002664; b) Z. Meng, A. Aykanat, K. A. Mirica, *J. Am. Chem. Soc.* **2019**, *141*, 2046.

[8] a) G. Wu, J. Huang, Y. Zang, J. He, G. Xu, *J. Am. Chem. Soc.* **2017**, *139*, 1360; b) H. Arora, R. Dong, T. Venanzi, J. Zscharschuch, H. Schneider, M. Helm, X. Feng, E. Cánovas, A. Erbe, *Adv. Mater.* **2020**, *32*, 1907063.

[9] X. Song, X. Wang, Y. Li, C. Zheng, B. Zhang, C. Di, F. Li, C. Jin, W. Mi, L. Chen, W. Hu, *Angew. Chem. Int. Ed.* **2020**, *59*, 1118.

[10] K. W. Nam, S. S. Park, R. dos Reis, V. P. Dravid, H. Kim, C. A. Mirkin, J. F. Stoddart, *Nat. Commun.* **2019**, *10*, 4948.

[11] a) R. A. Murphy, L. E. Darago, M. E. Ziebel, E. A. Peterson, E. W. Zaia, M. W. Mara, D. Lussier, E. O. Velasquez, D. K. Shuh, J. J. Urban, J. B. Neaton, J. R. Long, *ACS Cent. Sci.* **2021**, *7*, 1317; b) X. Huang, P. Sheng, Z. Tu, F. Zhang, J. Wang, H. Geng, Y. Zou, C. Di, Y. Yi, Y. Sun, W. Xu, D. Zhu, *Nat. Commun.* **2015**, *6*, 7408; c) J.-H. Dou, L. Sun, Y. Ge, W. Li, C. H. Hendon, J. Li, S. Gul, J. Yano, E. A. Stach, M. Dincă, *J. Am. Chem. Soc.* **2017**, *139*, 13608; d) R. W. Day, D. K. Bediako, M. Rezaee, L. R. Parent, G. Skorupskii, M. Q. Arguilla, C. H. Hendon, I. Stassen, N. C. Gianneschi, P. Kim, M. Dincă, *ACS Cent. Sci.* **2019**, *5*, 1959; e) G. Skorupskii, K. N. Le, D. L. M. Cordova, L. Yang, T. Chen, C. H. Hendon, M. Q. Arguilla, M. Dincă, *Proc. Natl. Acad. Sci. USA* **2022**, *119*, e2205127119; f) Y. Chen, Q. Zhu, K. Fan, Y. Gu, M. Sun, Z. Li, C. Zhang, Y. Wu, Q. Wang, S. Xu, J. Ma, C. Wang, W. Hu, *Angew. Chem. Int. Ed.* **2021**, *60*, 18769.

[12] a) Z. Meng, C. G. Jones, S. Farid, I. U. Khan, H. M. Nelson, K. A. Mirica, *Angew. Chem. Int. Ed.* **2022**, *61*, e202113569; b) C. Yang, R. Dong, M. Wang, P. St. Petkov, Z. Zhang, M. Wang, P. Han, M. Ballabio, S. A. Bräuninger, Z. Liao, J. Zhang, F. Schwotzer, E. Zschech, H.-H. Klauss, E. Cánovas, S. Kaskel, M. Bonn, S. Zhou, T. Heine, X. Feng, *Nat. Commun.* **2019**, *10*, 3260.

[13] a) R. Dong, P. Han, H. Arora, M. Ballabio, M. Karakus, Z. Zhang, C. Shekhar, P. Adler, P. St. Petkov, A. Erbe, S. C. B. Mannsfeld, C. Felser, T. Heine, M. Bonn, X. Feng, E. Cánovas, *Nat. Mater.* **2018**, *17*, 1027; b) Y. Yue, P. Cai, X. Xu, H. Li, H. Chen, H. Zhou, N. Huang, *Angew. Chem. Int. Ed.* **2021**, *60*, 10806.

[14] a) L. M. Malard, M. A. Pimenta, G. Dresselhaus, M. S. Dresselhaus, *Phys. Rep.* **2009**, *473*, 51; b) Z. Wang, G. Wang, H. Qi, M. Wang, M. Wang, S. W. Park, H. Wang, M. Yu, U. Kaiser, A. Fery, S. Zhou, R. Dong, X. Feng, *Chem. Sci.* **2020**, *11*, 7665.

[15] Z. Wang, L. S. Walter, M. Wang, P. S. Petkov, B. Liang, H. Qi, N. N. Nguyen, M. Hambsch, H. Zhong, M. Wang, S. Park, L. Renn, K. Watanabe, T. Taniguchi, S. C. B. Mannsfeld, T. Heine, U. Kaiser, S. Zhou, R. T. Weitz, X. Feng, R. Dong, *J. Am. Chem. Soc.* **2021**, *143*, 13624.

[16] D. Briggs, G. Beamson, *Anal. Chem.* **1993**, *65*, 1517.

[17] X. Chen, X. Wang, D. Fang, *Fullerenes Nanotubes Carbon Nanostruct.* **2020**, *28*, 1048.

[18] Y. Misumi, A. Yamaguchi, Z. Zhang, T. Matsushita, N. Wada, M. Tsuchiizu, K. Awaga, *J. Am. Chem. Soc.* **2020**, *142*, 16513.

[19] T. Yang, T. Willhammar, H. Xu, X. Zou, Z. Huang, *Nat. Protoc.* **2022**, *17*, 2389.

[20] Deposition Number 2237143 contains the supplementary crystallographic data for this paper. These data are provided free of charge by the joint Cambridge Crystallographic Data Centre and Fachinformationszentrum Karlsruhe Access Structures service.

[21] A. Kuc, M. A. Springer, K. Batra, R. Juarez-Mosqueda, C. Wöll, T. Heine, *Adv. Funct. Mater.* **2020**, *30*, 1908004.

[22] R. Ulbricht, E. Hendry, J. Shan, T. F. Heinz, M. Bonn, *Rev. Mod. Phys.* **2011**, *83*, 543.

[23] T. L. Cocker, D. Baillie, M. Buruma, L. V. Titova, R. D. Sydora, F. Marsiglio, F. A. Hegmann, *Phys. Rev. B* **2017**, *96*, 205439.

Manuscript received: January 4, 2023
Accepted manuscript online: March 2, 2023
Version of record online: ■■, ■■

Research Articles

Metal-Organic Frameworks

L. Sporrer, G. Zhou, M. Wang, V. Balos, S. Revuelta, K. Jastrzembski, M. Löffler, P. Petkov, T. Heine, A. Kuc,* E. Cánovas,* Z. Huang,* X. Feng,* R. Dong*

Near IR Bandgap Semiconducting 2D Conjugated Metal-Organic Framework with Rhombic Lattice and High Mobility

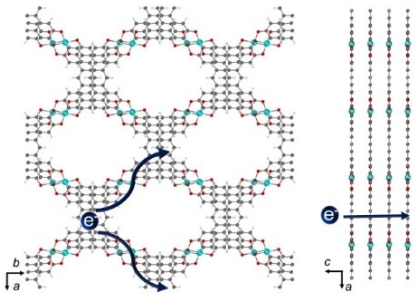

High-mobility 2D *c*-MOF semiconductor

The first rhombic 2D conjugated metal–organic framework (2D *c*-MOF) single crystal (named **Cu_2(OHPTP)**) is achieved based on a novel octahydroxyphenanthro[9,10:b]triphenylene ligand. **Cu_2(OHPTP)** is an intrinsic *p*-type semiconductor with a band gap of 0.5 eV and charge carrier mobility as high as $\approx$10.0 $cm^2 V^{-1} s^{-1}$.